Extracting Quasiparticle Lifetimes from STM experiments

Sumiran Pujari
*Department of Physics, Cornell University, Ithaca, New York 14853-2501**

Based on Quasiparticle interference(QPI) around a point impurity, we demonstrate an analysis scheme that extracts the lifetime of a quasiparticle by using the local density of states(LDOS) data around the impurity in a Scanning Tunneling Microscopy(STM) experiment. This data analysis scheme would augment the Fourier-Transform Scanning Tunneling Spectroscopic methods which provides us with the quasiparticle dispersion. Thus, point impurities can be *used* as probes to extract quasiparticle lifetimes from STM experiments and this would complement other experimental methods such as Angle Resolved Photo-emission Spectrocopy(ARPES). We detail how the scheme would apply to metals and superconductors.

Scanning Tunneling Microscopy(STM) has revolutionized condensed matter research by providing us with unprecedented detail on the local real space electronic properties of the sample under investigation. But even more remarkably, it has been shown that momentum space properties of the sample can be extracted through the application of Fourier Transform Scanning Tunneling Spectroscopy (FT-STS) [1]. Using FT-STS one figures out the dispersion of the underlying well-defined quasiparticles or carriers.

In this paper, we aim to extend the domain of momentum space properties that can be extracted using STM. The central result is the demonstration of a data analysis scheme that would give us the lifetimes of the charge carriers in a sample as a function of momentum(and energy) from data collected in an STM experiment. Previously, ARPES is the tool that has been used successfully to extract lifetimes of carriers in a sample by measuring the one-particle electron spectral function directly in momentum space. Extracting lifetime information from STM - a real space probe - thus would add value by providing an independent method that complements and checks the ARPES method. Previous attempts at reconciling lifetime broadening effects on STM data mainly consist of writing down viable fitting forms for the lifetime function that fit with the STM data, rather than extracting it out of the data directly like one does in an ARPES experiment by quantifying the width of the peaks in ARPES spectra (See e.g. [2]). In the context of metals/Fermi liquids, Ref. [3] have fitted STM data on Silver and Copper with a model for thermal broadening of the electrons [4]. Refs. [5] and [6] are prominent examples in the STM phenomenology of high temperature superconductors.

We start by describing the scheme in the simpler case of normal metals. We imagine the system to be composed of Landau quasiparticles described by a propagator of the form

$$\tilde{G}_0(k;\omega) = \frac{1}{\omega - i\eta(k,\omega) - \epsilon(k)} \tag{1}$$

Self-energy processes - e.g. due to electron-electron interaction as in a Fermi Liquid or through scattering off a bosonic mode like phonons - lead to a finite lifetime for the quasiparticle and this is formally taken care by the imaginary term in the denominator of Eq. (1), $\eta(k,\omega)$. Also, the real part of the self-energy shifts the chemical potential and we assume that the dispersion term $\epsilon(k)$ is this shifted dispersion [7]. Our aim is to extract $\eta(k,\omega)$ from STM data. We assume the knowledge of the dispersion $\epsilon(k)$ either via FT-STS on the same data or through an ARPES experiment.

Apart from the quasiparticles, let us imagine there to be a point impurity in the system, say at origin, which scatters the quasiparticles. In a real situation, we are imagining there to be a dilute amount of impurities in the sample so that multiple impurity scattering is not important. The impurity problem is solved via the T-matrix approach [8], and the real space impurity scattered electron propagator is given by

$$G(r,r';\omega) = G_0(r,r';\omega) + G_0(r,r_{imp};\omega)\cdot T(\omega)\cdot G_0(r_{imp},r';\omega) \tag{2}$$

where $G_0(r,r';\omega) = (2\pi/L)^2\sum_k \tilde{G}_0(k;\omega)e^{ik.(r-r')} \equiv G_0(R=r-r';\omega)$ is the free electron propagator and the impurity effect is captured by the so-called "T-matrix" $T(\omega)$, which is given by $T(\omega) = U/(1-UG_0(r_{imp},r_{imp};\omega))$ where U is the impurity strength. It is in the second term of the above equation that we have QPI which is utilized in FT-STS.

We will quickly review the key notions underlying FT-STS, since our method also utilizes QPI. STM measures LDOS as a spatial map over the surface for a range of energies. The LDOS $n(r;\omega)$ is proportional to imaginary part of the real space propagator, i.e.

$$n(r;\omega) = -\frac{1}{\pi}Im[G(r,r;\omega)]. \tag{3}$$

FT-STS's main operating principle is that the peaks in the Fourier transform of LDOS map at a particular energy are at wave-vectors which connect pairs of points on the $\epsilon(k)$'s contour at that particular energy for which the joint density of states is

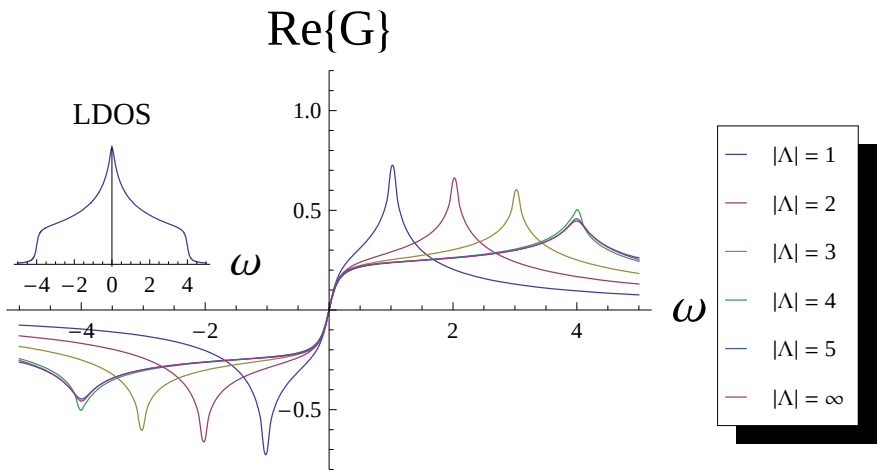

FIG. 1: In this figure, we demonstrate the effect of Kramers-Kroning to an example LDOS where we limit the integral by a finite cut-off, $Re[G(r,r;\omega)] = P\int_{-\Lambda}^{\Lambda} \frac{n(r,r;x)}{(\omega-x)}$. The example LDOS (see inset) is for a nearest-neighbour hopping model at half-filling, $\tilde{G}_0(k;\omega) = (\omega - i0.1t + 2t(Cos[k_x] + Cos[k_y]))^{-1}$ and $t = 1$. Around the Fermi energy($\omega = 0$ in this case), we see that even for $|\Lambda| = 3$, $Re[G]$ agrees well upto around $|\omega| = 1$. One can quantitatively show that this error is at most $Log|\frac{\Lambda+\omega}{\Lambda-\omega}| \approx 2|\omega/\Lambda|$ in units of n and we do much better than that(see Supplementary).

maximum. This can be understood by looking at the Fourier transform of the interference term in Eq. (2) (see Eq. (1) of [9] and the following paragraph). If the quasiparticles have finite lifetimes, the resultant effect in FT-STS will be a broadening of the FT-STS peaks(which are seen in experiments, e.g. [10]). Moreover, the "shapes" of these FT-STS peaks contain information about the momentum dependence of the lifetime $\eta(k;\omega)$. It seems that extracting the k-dependence of $\eta(k;\omega)$ from the FT-STS method is a hard task because, apart from other possible broadening factors like inhomogeneity (e.g. STM on cuprates), one has the difficulty of deconvolving the output of FT-STS - the QPI term is a product in real space - without the prior knowledge of $\eta(k;\omega)$. Instead we will work in real space, our main tactic being to extract $G_0(R;\omega)$ from QPI, and STM data is most suited for this.

We now list down the main steps of the analysis scheme and in what follows we give their essential technicalities along with pictorial demonstrations. In the Appendix, we include further technical details and proofs required in those steps. 1) From LDOS/$n(r;\omega)$ map, we construct a $G(r,r;\omega)$ map. 2) Once we have the $G(r,r;\omega)$ data, we "invert" Eq. (2) in order to extract $G_0(R;\omega)$. To invert Eq. (2), we need 2a) a way to find $G_0(R=0;\omega)$ and 2b) a way to find the correct phases of $G_0(R;\omega)$. Once this is done, we Fourier transform to get $\tilde{G}_0(k;\omega)$ and, thence, $\eta(k;\omega)$. We show results of this method for various cases of dispersion and lifetimes. Then, we discuss what kind of data sets are desirable and how the method extends to the superconducting case.

The first step of the analysis method is to convert the LDOS data to $G(r,r;\omega)$. This will be achieved through a Kramers-Kronig relation the propagator satisfies, $Re[G(r,r;\omega)] = P\int n(r,r;x)/(\omega - x)$ where the principle value integral is over the real line. Since the LDOS is nonzero only within a finite bandwidth [11], this integral is over a finite range of energies. In general, in a real experiment one might have information only over part of the bandwidth in which case, we can definitively apply this method only to an energy range that is well within the measured energy range, where even the incomplete spectrum can be fruitfully used as demonstrated in Fig. 1. This is very often the/one of the interesting energy ranges(e.g. around the Fermi energy for metals or the nodal energy for cuprates). We can also apply some form of extrapolation to construct LDOS data over the full bandwidth [12]. Kramers-Kronig has been applied successfully to other spectroscopies, e.g. Electron Microscopy (see [13]), thus giving us reason that they be applied to STM data as well.

We now discuss the second step : how to invert Eq. (2) at a fixed energy. We are only concerned with $r = r'$. We set $r_{imp} = 0$. The first step is to find out the first term on the right hand side of Eq. (2), $G_0(R=0;\omega)$. This will be done through a minimization procedure where a cost function would penalize incorrect guesses for $G_0(0;\omega)$. Given a $G_0(0;\omega)$ guess(which is independent of R if the free propagator is that of a translationally invariant system), we can solve for $T(\omega)$ by solving Eq. (2) for $r = r' = r_{imp}$ (Furthermore, we can calculate the impurity strength U from $T(\omega)$). Once $T(\omega)$ is known, we can solve for $G_0(R;\omega)$ as

$$G_0(R;\omega) = \sqrt{\frac{G(r,r;\omega) - G_0(0;\omega)}{T(\omega)}} \tag{4}$$

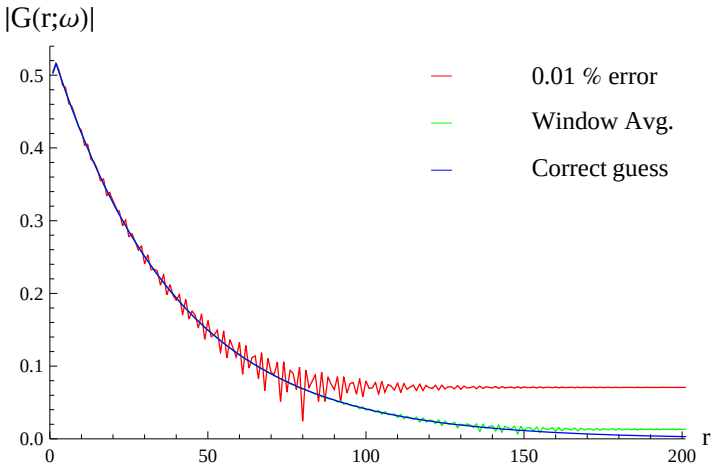

FIG. 2: Above is shown $|G_0(R;\omega)|$ on a 200-site window around an impurity extracted with various start guesses for $G_0(0;\omega)$.

In Green's function theory, one can show that the magnitude $|G_0(R;\omega)|$ monotonically decays to zero for large R (exponentially in R in one dimensions and as square root of R in two dimensions, see Supplementary) for dispersion that have convex energy contours. We demonstrate this effect in 1D and also show the effect of incorrect $G_0(0;\omega)$ on extracted $|G_0(R;\omega)|$ in Fig. 2. We see how an incorrect guess for $G_0(0;\omega)$ spoils the monotonic decay of $|G_0(R;\omega)|$. The reason for the deviation from monotonicity is as follows : Given our (incorrect) guess of $|G_0(0;\omega)|$, we can decompose the incorrect $G_0(R;\omega)$ as $G_0^{correct}(R;\omega) + G_0^{error}$ where G_0^{error} is a constant. Therefore, $|G_0(R;\omega)| = |G_0^{correct}(R;\omega)| + |G_0^{error}| + 2|G_0^{correct}(R;\omega)||G_0^{error}| \times Cos(Arg[G_0^{correct}(R;\omega)] - Arg[G_0^{error}])$, and it is the final cosine term in the above expression which spoils the monotonicity even for large R. Moreover, the $|G_0^{error}|$ term would also not let the Green's function decay to zero as $r \to \infty$. This motivates a minimization using a cost function that penalizes deviation from the smooth decay of extracted $|G_0(R;\omega)|$ for finding the correct $|G_0(0;\omega)|$ [14]. A good start guess for $G_0(0;\omega)$ is to take a spatial average of $G(r,r;\omega)$ over the whole data set around the impurity. One can show that the error in the guessed $G_0(0;\omega)$ is $1/L^2$($1/L^d$ in d dimensions, see Supplementary) suppressed compared to the guessed $G_0(0;\omega)$, and if the window were infinite, the spatial average of $G(r,r;\omega)$ would exactly equal $G_0(0;\omega)$.

With the correct $G_0(0;\omega)$, we still get $G_0(R;\omega)$ only up to a phase of π. Capturing this phase is crucial to get the correct $\tilde{G}_0(k;\omega)$ upon Fourier transforming. To get the correct phase, we start with the observation that the phases have to be smooth and well-behaved as a function of R because $G_0(R;\omega)$ is differentiable with respect to R [15]. We use this property to fix the phase of the square of $G_0(R;\omega)$, i.e. we select that branch of the argument function when evaluating the phase of $G_0(R;\omega)^2$ which maintain the aforesaid smoothness. We start by making a spatial list of the phases as given by the $Arg(z)$ function which restricts the phase obtained to one branch of the Argument function. Then, we start at $R = 0$. As we move away from the origin, we multiply phase factors of $e^{i2m\pi}$ to $G_0(R;\omega)^2 = |G_0(R;\omega)^2|e^{i\phi_{principal}}$ for all R, the m's being so chosen that if $|R'| > |R|$ then $\phi'_{principal} + 2\pi m' > \phi_{principal} + 2\pi m$. Once that is done, the phase of $G_0(R;\omega)$ is just half that of $G_0(R;\omega)^2$. We demonstrate the working of this phase reconstruction method in Fig. 3 (see Supplementary for a flowchart of the method).

With the correct phases, we are now ready to Fourier transform the extracted $G_0(R;\omega)$ to get $\tilde{G}_0(k;\omega)$ and $\eta(k;\omega)$ with our knowledge of $\epsilon(k)$. Moreover, the extracted $\tilde{G}_0(k;\omega)$ also has to satisfy the exclusive momentum dependence of $\omega - Re[\tilde{G}_0(k;\omega)^{-1}]$. In Fig. 4, we show how this method performs with and without error and we see that it performs well for error magnitudes less than 0.25 %. For the panels Fig. 4 a-d, the form of η had no momentum dependence, and this kind of fitting form has been proposed in [6] for Cuprates and has been theoretically discussed in [16]. In general, we expect the lifetime function to have few (low) harmonics of k similar to the dispersion. Thus, our analysis scheme would serve the purpose of finding the most general $\eta(k;\omega)$ that is consistent with STM data. We can extract an approximate analytic form for η by doing a least-squares fit of the extracted η to a function of k containing a few harmonics in the Brillouin zone. The approximate analytic form can then be compared to theoretical proposals.

At this point, we comment on what kind of data sets would be ideal for such an analysis. In Fig. 5, we show an example of data set seen in a real experiment. We show how it is similar to a theoretical data set(calculated numerically) which has a lifetime broadening. Thus, we would expect that if we observe a few of the "Friedel oscillation"-like rings around the point impurity, this analysis scheme should work. Moreover, if FT-STS applied to a single point impurity data shows reliable QPI peaks, then we believe that the data set would have good enough spatial resolution to resolve the momentum dependence of lifetime η to the same momentum resolution as that of the FT-STS results. We can improve on this by taking an average over

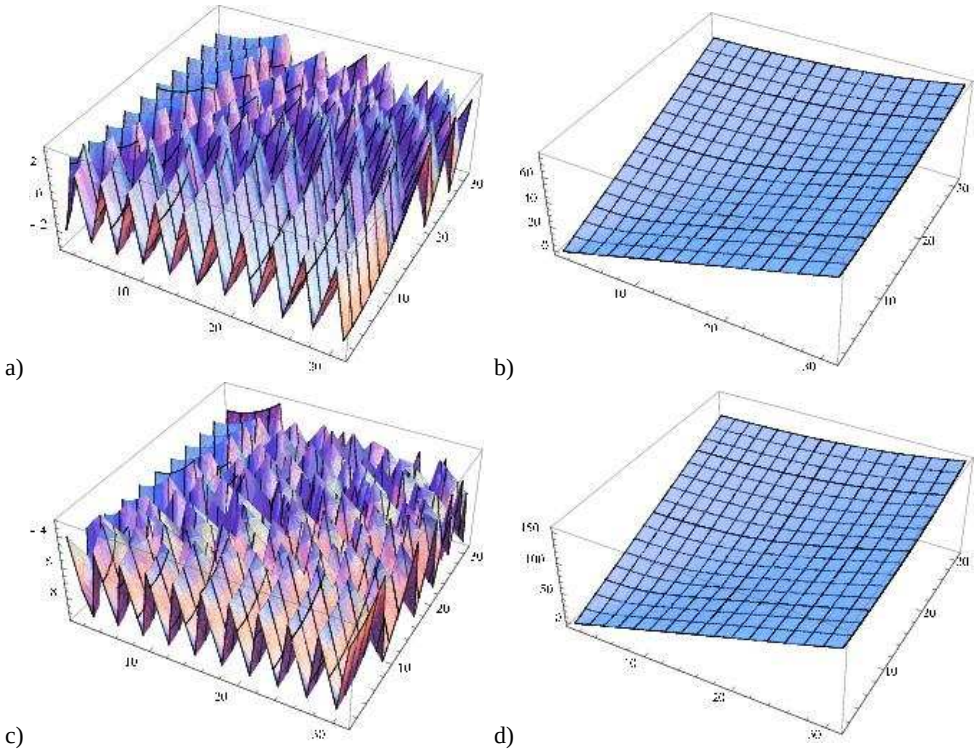

FIG. 3: In the panels above we show the phases of $G_0(R;\omega)$ (a) and b)) and $G_0(R;\omega)^2$ (c) and d)) in the first quadrant of size 30x30 lattice sites around an impurity at a fixed $\omega(=-t)$. a) and c) show the phases as evaluated by the Arg(z) function restricted to one branch. b) and d) show the smooth phases as reconstructed using the reconstruction algorithm. The ratio of phases in b) and d) is identically two over the whole quadrant, even though the ratio of phases in a) and c) does not behave in such a regular manner. $\epsilon(k) = -2t(Cos[k_x] + Cos[k_y])$ and $\eta(k, \omega = -t) = 0.1t$ in this example.

data sets around multiple point impurities to improve signal to noise. Now, we will sketch how this method of analysis can be extended to superconducting case using d-wave superconductors(pertinent to Cuprate phenomenology) as our example. In Nambu's two component notation, the free superconducting propagator looks like

$$\tilde{G}_0(k;\omega)^{-1} = \begin{pmatrix} \omega - i\eta_e(k,\omega) - \epsilon(k) & \Delta(k) \\ \Delta(k)* & \omega - i\eta_h(k,\omega) + \epsilon(k) \end{pmatrix} \tag{5}$$

where $\epsilon(k)$ is the bare dispersion and $\Delta(k)$ is the (d-wave) gap of the cuprate in question. These are assumed to be known(through other experiments). As before, we want to determine the electron/hole lifetime. The first simplification is the relation $\eta_h(k,\omega) = -\eta_e(k,-\omega)$. The proof of this relation in outlined in the supplementary information to this manuscript and it follows by showing $\Sigma_{22}(-\omega - i\delta) = -\Sigma_{11}(\omega + i\delta)$. This relation implies $G_0(R,\omega)_{22} = -G_0(R,-\omega)_{11}$ and $G_0(R,\omega)_{12} = G_0(R,-\omega)_{12}$. Now, as before, we imagine there is a point impurity which result in a two-component T-matrix. One can show that this T-matrix has no off-diagonal entries(for an ordinary potential impurity) since $G_0(R=0,\omega)_{12} = 0$ owing to the d-wave symmetry of the gap function. One can further show that $T_{22}(-\omega) = -T_{11}(\omega)$ and, resultantly, $G(r,r;\omega)_{22} = -G(r,r;-\omega)_{11}$. For $r = r_{imp}$, we have $G_{11} = G_{0,11} + T_{11}G^2_{0,11}$ and $G_{22} = G_{0,22} + T_{22}G^2_{0,22}$. Using $G(r,r;,\omega)_{22} = -G(r,r;,-\omega)_{11}$, we can thus determine T_{11} and T_{22} given a guess for $G_0(R=0,\omega)_{11}$ (which will again be determined by demanding the monotonicity of $G_0(R,\omega)_{11}$). For $r \neq r_{imp}$, we have

$$\begin{aligned} G_{11}(r,r;\omega) &= G_0(0,\omega)_{11} + T_{11}(\omega)G_0(r-r_{imp},\omega)^2_{11} \\ &\quad + T_{22}(\omega)G_0(r-r_{imp},\omega)_{12}G_0(r-r_{imp},\omega)_{21} \end{aligned} \tag{6}$$

$$\begin{aligned} G_{22}(r,r;\omega) &= G_0(0,\omega)_{22} + T_{22}(\omega)G_0(r-r_{imp},\omega)^2_{22} \\ &\quad + T_{11}(\omega)G_0(r-r_{imp},\omega)_{12}G_0(r-r_{imp},\omega)_{21}. \end{aligned} \tag{7}$$

Again using $G(r,\omega)_{22} = -G(r,-\omega)_{11}$, now with the knowledge of T_{11} and T_{22}, we can solve the above equations for $G_0(R,\omega)$ upto a phase of π (which we reconstruct as before) at each ω for all r in the dataset, following which we Fourier transform to extract $\tilde{G}_0(k,\omega$ and $\eta_e(k,\omega)$.

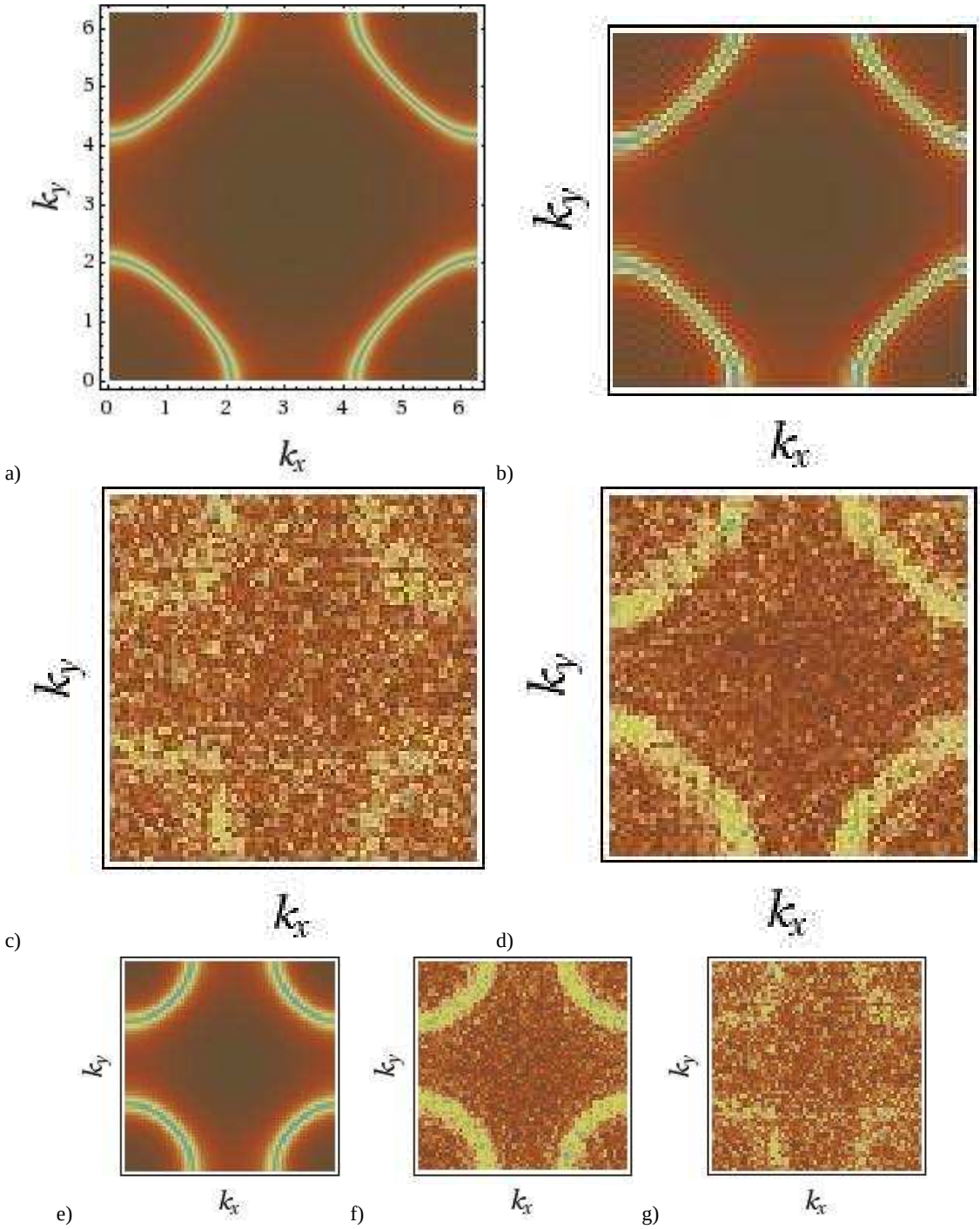

FIG. 4: In these figures we are plotting $|(\omega + i\eta(k,\omega) - \epsilon(k))^{-1}|$ as a function of $\vec{k}$ over a Brillouin Zone $(0, 2\pi) \times (0, 2\pi)$ at a fixed $\omega(= -t$ for the above plots). In a) we show the input form resulting out of our choice of input for η, where $\epsilon(k) = -2t(Cos[k_x] + Cos[k_y])$ (nearest-neighbour hopping) and $\eta(k, \omega = -t) = 0.1t$; in b) we show the form extracted using the proposed analysis scheme when no noise was added to the STM data calculated numerically. One sees the limitation in momentum resolution in the form of "blockiness" introduced by having a finite window. This "blocky" momentum resolution gets better or worse with greater or smaller window sizes. In c) and d) we show the results of the analysis scheme to data with 1% and 0.05% Gaussian errors added respectively. We have done similar analyses for different energy values and different forms of η and in e), f) and g), we show the corresponding results for $\epsilon(k) = -2t(Cos[k_x] + Cos[k_y]) - 4(0.2t)(Cos[k_x] * Cos[k_y])$ (nearest and second-nearest neighbour hopping) and $\eta(k, \omega = -t) = 0.25t + 0.1t(Cos[k_x] + Cos[k_y])$ as another example.

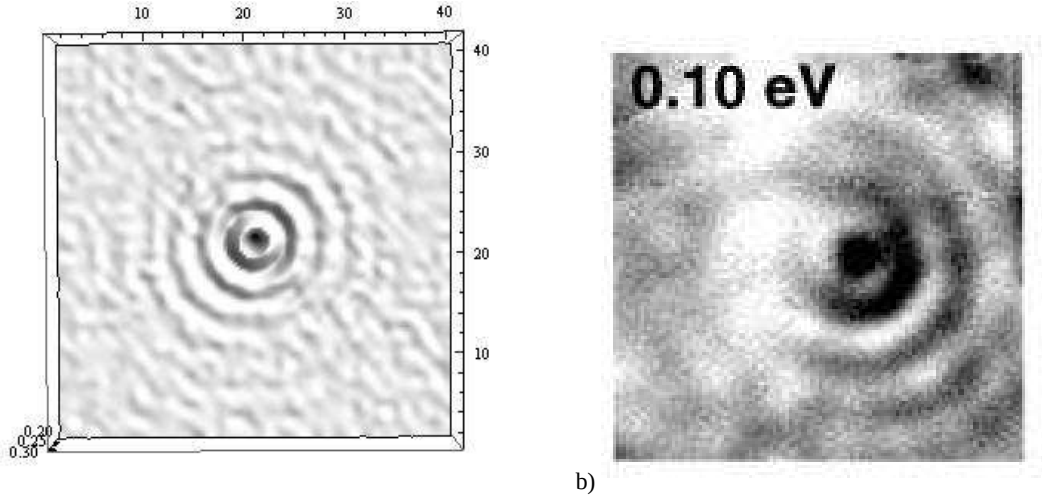

a) b)

FIG. 5: In this figure we compare an experimental data set on InAs surface(taken from [17] with due permission from APS and the authors) with a numerically calculated LDOS data set with error 0.5 % added. This figure serves to illustrate that there exist data sets, perhaps within operable error range, to which the scheme can potentially be applied.

In conclusion, we demonstrated an analysis scheme which holds promise to extract lifetimes from STM data in various systems ranging from metals and semiconductors to strongly correlated compounds to superconductors. Some final remarks are in order. We demonstrated the proposed analysis scheme in case of a point impurity, but it can be extended to the case of an extended impurity too. The resulting complication will be that now we would have to guess more than just $G_0(R=0;\omega)$ (e.g. if the impurity extends over two adjoining sites r_1 and r_2, then $G(r,r;\omega)$ will be a function of $G_0(0;\omega) = G_0(r_1,r_1;\omega) = G_0(r_2;r_2;\omega)$ and $G_0(1;\omega) = G_0(r1,r2;\omega)$). This scheme is inherently local, where we would be analyzing data around a single impurity. Thus, it would really utilize the local information that STM affords us with. There have been other examples of data analysis done on STM data previously to extract localinformation([18],[19]). In this sense, we would do better than ARPES where the signal is averaged over an area of the sample equal to the beam size, iff the STM experiment has good signal to noise. Similarly, we can overcome inhomogeneity issues for dirty systems, in which case we would concentrate this analysis on a homogeneous patch similar in spirit to Hudson's analysis [19] and to a previous work [20].

Acknowledgements : This work has been supported by the NSF grant DMR-0552461. I acknowledge the extremely valuable suggestions of C. L. Henley, especially regarding the checks on robustness of the method to error and phase fixing, and a critical reading of the manuscript. I also thank him and H. J. Changlani, Milan Allan and J. C. Davis for helpful discussions.

APPENDIX : SUPPLEMENTARY INFORMATION

Limit on the Error introduced by Kramers-Kroning Integration

The Kramers-Kronig relation relates the real part of a Green's function to the imaginary part as follows

$$Re[G(r,r;\omega)] = -\frac{1}{\pi}P\int_{-\infty}^{\infty} dx \frac{Im[G(r,r;x)]}{(\omega - x)} = P\int_{-\infty}^{\infty} dx \frac{n(r;x)}{(\omega - x)}. \tag{8}$$

If we limit the integral by cut-offs Λ_+ and Λ_-, then the error E introduced is

$$P\int_{-\infty}^{\Lambda_-} dx \frac{n(r;x)}{(\omega - x)} + P\int_{\Lambda_+}^{\infty} dx \frac{n(r;x)}{(\omega - x)}. \tag{9}$$

Even if we were to make the really bad approximation that $n(r;x) = n(r;\omega)$ for all x (and this is a really bad approximation, since $n(r;x)$ decays to zero as $x \to \infty$), we get

$$E < n(r;\omega) Log \frac{|\omega - \Lambda_-|}{|\omega - \Lambda_+|} \tag{10}$$

since $n(r;x) > 0$ for all x. Thus, if $\omega/\Lambda_- << 1$ and $\omega/\Lambda_+ << 1$, then the error in $Re[G(r,r;\omega)]$ is less than $n(r,\omega) * (\frac{\omega}{\Lambda_+} + \frac{\omega}{\Lambda_-} + Log\frac{|\Lambda_-|}{|\Lambda_+|})$. Since, $Re[G(r,r;\omega)]$ and $n(r;\omega)$ carry the same dimensions and $n(r;\omega) < 1$, this is at most an $O(\frac{|\omega|}{|\Lambda|})$ error.

Proof of Monotonic decay of $G_0(\vec{R};\omega)$ for large $\vec{R}$

In two dimensions, $G_0(\vec{R})$ on a lattice is given by the formula

$$\begin{aligned} G_0(\vec{r},\vec{r}_{imp};\omega) &\equiv G_0(\vec{r}-\vec{r}_{imp};\omega) = G_0(\vec{R};\omega) \\ &= \lim_{\delta\to 0^+}\frac{1}{(2\pi)^2}\int_{B.Z.} d\vec{k}\frac{e^{i\vec{k}.\vec{R}}}{\omega+i\delta-\epsilon(\vec{k})} \\ &= \frac{1}{(2\pi)^2}\int_{-\pi}^{\pi} dk_x e^{ik_xR_x}\int_{-\pi}^{\pi} dk_y \frac{e^{ik_yR_y}}{\omega+i\delta-\epsilon(\vec{k})} \end{aligned} \tag{11}$$

Let us look at the k_y integral for a particular k_x. The denominator vanishes for certain values of k_y thus motivating the conversion of the k_y integral to a contour integral. The mapping $z=e^{ik_y}$ achieves the conversion which also maps the integral from $-\pi$ to π to a contour integral over the unit circle. The periodicity of the integrand over the zone ensures the analyticity of the resulting complex integrand. Thus,

$$G_0(\vec{R};\omega) = \frac{1}{(2\pi)^2}\int_{-\pi}^{\pi} dk_x e^{ik_xR_x}\oint_{U.C.}\frac{dz}{iz}\frac{z^{R_y}}{\omega+i\delta-\epsilon(k_x,z)} \tag{12}$$

For a particular ω energy contour and k_x, we get two poles (See Fig.). Expanding the denominator around the poles gives us $\omega+i\delta-\epsilon(k_x,z) = -\frac{\hbar v_{g_y}(\omega,k_x)}{iz_p}(z-z_p(1-\frac{\delta}{\hbar v_{g_y}(\omega,k_x)}))$. The poles z_ps are defined by $\epsilon(k_x,z_p)=\omega$ and $\hbar v_{g_y}(\omega,k_x)\equiv\frac{\partial\epsilon(\vec{k})}{\partial k_y}$ is the group velocity along y direction. We need only worry about the $(z-z_p)$ term in the expansion of the denominator since other expansion terms will yield zero residues. From the $(1-\frac{\delta}{\hbar v_{g_y}(\omega,k_x)})$ factor in the expansion, we realize that the pole where the sign of the $\hbar v_{g_y}$ is same as the positive δ will be "pulled" inside the unit circle while the other pole will be "pushed" out of the unit circle. Thus, when we do k_x integral, only one half of the ω *energy* contour (not to be confused with the complex contour; to distinguish we will call ω contours as energy contours) will contribute to the integral. In the process, we have converted the 2D integral over the zone into an integral over part of the energy contour. Filling in the steps,

$$\begin{aligned} G_0(\vec{R};\omega) &= \frac{1}{(2\pi)^2}\int_{-\pi}^{\pi} dk_x e^{ik_xR_x}\oint_{U.C.}\frac{dz}{iz}\frac{z^{R_y}}{-\frac{\hbar v_{g_y}(\omega,k_x)}{iz_p}(z-z_p(1-\frac{\delta}{\hbar v_{g_y}(\omega,k_x)}))} \\ &= -\frac{1}{(2\pi)^2}\int_{-\pi}^{\pi} dk_x e^{ik_xR_x}2\pi i\frac{z_p^{R_y}}{\hbar v_{g_y}(\omega,k_x)} \\ &= -\frac{1}{(2\pi)^2}2\pi i\int dk_x\frac{e^{ik_xR_x}e^{ik_{y_p}(\omega,k_x)R_y}}{\hbar v_{g_y}(\omega,k_x)} \\ &= \frac{1}{2\pi i}\oint_{\mathrm{sgn}(\delta)=\mathrm{sgn}(\mathrm{v_{g_y}(\omega,s)})} ds\frac{e^{i\vec{k}(s,\omega).\vec{R}}}{|\nabla\epsilon(\vec{k}(s,\omega))|} \end{aligned} \tag{13}$$

where the last step was achieved by converting the element dk_x to a parameter s characterising the ω energy contour and we integrate over that part of the contour where the sign of δ is same as v_{g_y}.

For large $\vec{R}$, i.e. far from impurity, we notice that the phase $e^{i\vec{k}(s,\omega).\vec{R}}$ varies rapidly and thus stationary phase approximation can be applied. The phase factor is stationary at points on the energy contour where the group velocity is along the $\vec{R}$ direction since $d(\vec{k}(s,\omega).\vec{R})/ds = \vec{R}.d\vec{k}(s,\omega)/ds = 0$ only when $\vec{R}$ is perpendicular to $d\vec{k}(s,\omega)/ds$ and $d\vec{k}(s,\omega)/ds$, being the tangent to the energy contour, is perpendicular to the group velocity. Therefore,

$$G_0(\vec{R};\omega) = \frac{e^{i\pi/4}}{2\pi i}\frac{1}{|\nabla\epsilon(\vec{k}_{dom}(\vec{R},\omega))|}\sqrt{\frac{2\pi}{|\vec{R}||d^2\vec{k}(s,\omega)/ds^2|_{\vec{k}_{dom}(\vec{R},\omega)}}}e^{i\vec{k}_{dom}(\vec{R},\omega)\cdot\vec{R}} \tag{14}$$

where $\vec{k}_{dom}(\vec{R},\omega)$ is the $\vec{k}$ corresponding to which the group velocity at energy ω is along $\vec{R}$ and, thus, is a function of $\vec{R}$ (only through $\hat{R}$) and ω. For a convex dispersion function $\epsilon(\vec{k})$, we will have only one $\vec{k}_{dom}$ and thus

$$|G_0(\vec{R};\omega)| \propto \frac{1}{\sqrt{|\vec{R}|}} \tag{15}$$

for large $\vec{R}$. This proves the monotonic decrease of $G_0(\vec{R};\omega)$ when the lifetime is infinitesimal. When we have a finite lifetime due to self-energy processes, the propagator in momentum space looks like $\tilde{G}_0(\vec{k};\omega) = (\omega + i\delta - (\epsilon(\vec{k}) + i\eta(\vec{k},\omega)))^{-1}$ where the ω might have undergone a chemical potential shift, and the whole algebra in the above will go through similarly and we will get

$$|G_0(\vec{R};\omega)| \propto \frac{1}{\sqrt{|\vec{R}|}} e^{-\frac{\eta(\vec{k}_{dom}(\vec{R},\omega))}{|\nabla\epsilon(\vec{k}_{dom}(\vec{R},\omega))|}|\vec{R}|} \tag{16}$$

In one dimension, we only get the monotonic exponential decay for large $\vec{R}$.

IMPLEMENTATION OF COST FUNCTION FOR FINDING $G_0(R=0;\omega)$

As mentioned in the main manuscript, the Cost function for a one-dimensional list of values for $|G_0(R;\omega)|$ (that is extracted given a guess $G_0(R=0;\omega)$) was

$$Cost(\{z_r\}) = \sum_r \frac{|z_{r+1} + z_{r-1} - 2z_r|^2}{|(z_{r+1} + z_{r-1})/2|^2} \tag{17}$$

where the list is $\{z_r\}$ and sum runs over all 3-tuples. We generalize this to two dimension by evaluating the one-dimensional cost using the same formula for all one-dimensional slices of the two-dimensional data set either along x or y direction. We do it this way because the two-dimensional data set is symmetric with respect to interchanging x and y when there is no error. In the error-full case, we can pre-process the data set to impose the symmetries of the square lattice. Thus the Cost function is

$$Cost(\{z_{x,y}\}) = \sum_y \sum_x \frac{|z_{x+1,y} + z_{x-1,y} - 2z_{x,y}|^2}{|(z_{x+1,y} + z_{x-1,y})/2|^2} \tag{18}$$

We show the profile of this Cost function as a function of $G_0(R=0;\omega)$ guesses for the no-error case (which includes the numerical error incurred during two-dimensional Numerical Integration in Mathematica) and error-full cases in Fig. 6. We show it as a matrix where the center point(6,6) corresponds to the correct $G_0(R=0;\omega)$ and the (7,7)-entry corresponds to average over the $G(r,r;\omega)$ set (see next section). From point to point, we change the guess by $Re[Avg(G(r,r;\omega)) - G_0(R=0;\omega)]$ along x-direction and $Im[Avg(G(R;\omega)) - G_0(R=0;\omega)]$ along y direction. We see that in the no-error case, the Cost function has minimum at the correct value of $G_0(R=0;\omega)]$. In case of 0.1%, it does well to within $Avg(G(r,r;\omega)) - G_0(R=0;\omega)$. In case of 0.5%, it starts to seriously deviate and the best guess then would be $Avg(G(r,r;\omega))$.

A Good Guess for $G_0(r,r;\omega)$

Recalling that the T-matrix equation for scattering of point impurity is

$$G(r,r';\omega) = G_0(r,r';\omega) + G_0(r,r_{imp};\omega)\cdot T(\omega)\cdot G_0(r_{imp},r';\omega), \tag{19}$$

when we take the average of Eq. 19 with $r = r'$ over the window, the two terms on the right hand side average to(in two dimensions)

$$\frac{1}{L^2}\sum_r G_0(0;\omega) = (\frac{2\pi}{L})^2 \sum_k G_0(k;\omega) \tag{20}$$

$$\frac{1}{L^2}\sum_r G_0(r,0;\omega)T(\omega)G_0(0,r;\omega) = (\frac{2\pi}{L})^4 T(\omega)\sum_k G_0(k;\omega)^2 \tag{21}$$

$$\tag{22}$$

Thus, we see that the second term is $1/L^2$($1/L^d$ in d dimensions) suppressed compared to the first term, and if the window were infinite, the spatial average of $G(r,r;\omega)$ would exactly equal $G_0(0;\omega)$. For a finite but large enough window, it is a good guess for $G_0(0;\omega)$.

a)
```
539.238  517.192  480.558  455.357  483.146  526.168  532.907  481.578  479.351  479.911  510.442
500.72   497.939  458.983  405.208  412.83   422.243  419.665  402.611  427.597  462.664  514.964
506.821  464.844  380.628  339.749  306.183  315.05   314.686  323.685  391.342  450.975  517.702
470.296  409.648  320.441  258.852  183.675  169.546  193.139  267.715  358.469  464.87   507.947
465.888  411.166  309.891  187.925  82.9017  45.7886  86.9743  188.098  307.511  398.288  460.599
485.666  410.571  313.792  184.867  48.9257  3.5936   47.1426  162.098  278.544  382.236  432.65
521.963  460.674  337.781  223.156  88.8926  43.0211  92.7411  213.409  300.548  401.974  472.436
576.2    449.957  362.884  272.033  198.329  144.986  193.234  298.064  389.643  441.698  491.246
566.162  460.782  412.75   357.972  287.743  254.063  279.909  386.979  487.795  524.563  523.213
517.34   472.211  448.793  417.734  381.36   355.206  376.472  413.623  503.829  582.937  578.792
487.028  471.423  483.924  498.604  475.834  417.123  426.282  450.414  513.555  592.555  617.897
```

b)
```
581.865  565.535  554.349  561.683  548.3    556.993  598.945  661.841  647.138  617.003  619.641
590.513  569.113  552.095  531.317  531.274  559.229  595.314  651.293  631.701  636.191  648.253
616.954  589.803  551.794  524.224  516.649  550.219  592.995  607.17   613.045  702.882  669.748
639.416  610.027  578.469  526.832  499.443  512.808  547.834  530.749  582.625  710.503  645.552
645.325  648.301  608.452  567.35   505.849  476.692  483.789  484.806  535.06   590.926  637.148
664.955  700.321  634.724  582.189  514.757  452.253  438.86   454.124  501.073  556.25   613.204
689.518  744.853  620.959  541.026  498.365  458.653  439.113  453.436  519.962  559.975  577.771
665.557  644.157  602.54   552.118  502.903  477.294  470.276  506.134  523.295  550.928  574.724
655.917  635.459  610.326  562.764  530.082  518.215  522.233  561.17   569.449  606.031  598.648
623.632  617.58   618.168  610.082  559.48   538.606  550.546  586.173  612.755  604.402  603.033
610.287  630.03   657.41   642.103  599.747  575.798  594.722  622.91   662.804  625.179  609.922
```

c)
```
950.21   971.854  1009.56  1048.68  1079.02  1104.7   1133.77  1177.03  1186.42  1136.86  1097.61
974.27   993.663  1028.76  1090.11  1111.41  1112.89  1127.65  1174.47  1225.38  1138.88  1084.87
995.56   1017.91  1047.01  1094.52  1131.7   1132.41  1129.72  1141.61  1145.06  1121.37  1076.03
1014.62  1039.75  1071.92  1097.51  1129.12  1153.87  1136.98  1135.12  1126.52  1110.89  1082.94
1031.32  1063.33  1100.09  1122.42  1120.62  1141.09  1154.8   1151.3   1141.43  1125.42  1108.28
1049.12  1092.55  1124.93  1121.58  1123.57  1154.33  1193.98  1189.47  1174.21  1134.22  1103.21
1067.64  1113.28  1130.49  1118.21  1125.38  1160.22  1234.75  1240.27  1200.85  1141.13  1104.25
1076.79  1109.31  1117.12  1114.58  1123.91  1155.04  1218.19  1238.01  1187.94  1148.21  1116.37
1075.66  1092.29  1113.24  1114.93  1119.26  1139.    1172.23  1187.71  1164.77  1147.9   1114.95
1053.67  1081.83  1109.71  1104.79  1109.94  1120.85  1141.69  1148.69  1128.75  1103.89  1073.7
1038.97  1069.31  1102.85  1097.81  1100.67  1098.26  1102.28  1103.48  1083.33  1063.3   1041.13
```

FIG. 6: a) no-error, b) 0.1% error added and c) 0.5% error added to $G(r, r; \omega)$. In this example, $\epsilon(\vec{k}) = -2(Cos[k_x] + Cos[k_y])$ and $\eta(\vec{k}) = 0.1$ and $\omega = -1$ in unit of t.

Phase reconstruction algorithm

Here, we write down the flowchart for the phase reconstruction algorithm that is followed to fix the phase of $G_0(\vec{R}; \omega)$ which we get by taking the square root of the equation

$$G_0(\vec{R}; \omega)^2 = \frac{G(r, r; \omega) - G_0(\vec{R} = 0; \omega)}{G(r = 0, r = 0; \omega) - G_0(\vec{R} = 0; \omega)} * G_0(\vec{R} = 0; \omega))^2. \tag{23}$$

Upon taking the square root, we get $G_0(\vec{R}; \omega)$ upto a phase of $e^{i\pi}$. To fix this phase, we note that since the propagator in the continuum $G_0(\vec{R}; \omega)$ has to be a smooth well-behaved function for $\vec{R} \neq 0$ if it is to satisfy the Green's function equations of motion for the Hamiltonian operator and therefore its phase should also be a smooth and well-behaved as a function of $\vec{R}$. To see this we start with the equation of motion for the non-interacting case in the continuum is

$$(i\partial/\partial t + \nabla^2/2m)G_{non}(x, t; x', t') = \delta(x - x')\delta(t - t') \tag{24}$$

which upon Fourier transforming with respect to time gives

$$(\zeta + \nabla^2/2m)G_{non}(x, x'; \zeta) = \delta(x - x') \tag{25}$$

For $x \neq x'$, the above differential equation has no ill-behaved term and thus $G_{non}(x, x'; \zeta)$ has to be a well-behaved differentiable function. For the interacting case, the equations of motion is an infinite hierarchy of differential equations with the successive equations involving higher order Green's functions (See Vinay Ambegaokar's Chapter on The Green's Function Method in Superconductivity, Vol 1, edited by R. D. Parks). It is not clear to the author, how one could extend the non-interacting argument to this case. Instead, we argue as follows. As is usual in perturbation theory, the full propagator in momentum space

satisfies a Dyson's equation and is given by $\tilde{G}(\vec{p},\zeta) = (\zeta - p^2/2m - \Sigma(\vec{p};\zeta))^{-1}$ where $\Sigma(\vec{p};\zeta)$ is called the Self-energy and captures the effect of interactions. If this self-energy doesn't change the analytic structure of $\tilde{G}(\vec{p},\zeta)$ when compared to $\tilde{G}_0(\vec{p},\zeta)$ (More precisely, the pole at $\zeta = p^2/2m$ for the non-interaction survives, though it will get shifted off the real axis), then upon Fourier transforming to real space, the differentiability of $G(x,x';\zeta)$ will be preserved. Looking at Eq. 11's continuum version,

$$\nabla^2 G(\vec{R};\omega) = \lim_{\delta\to 0^+} \frac{1}{(2\pi)^2}\int_{B.Z.} d\vec{k} \frac{|\vec{k}|^2 e^{i\vec{k}.\vec{R}}}{\omega + i\delta - |\vec{k}|^2/2m - \Sigma(\vec{k};\omega)} \tag{26}$$

and if the pole structure of the integrand is same with and without Σ, then the differentiabiltity of $G_0(x,x';\zeta)$ implies differentiabiltity of $G(x,x';\zeta)$. In the case of a lattice, $G_0(\vec{R};\zeta)$ is well-behaved for $\vec{R} \neq 0$ and at $\vec{R} = 0$ there is a kink in its phase (See the origin in Fig. 7 b) and d)).

Similarly, $G_0(\vec{R};\omega)^2$'s phase should also be well-behaved as a function of space. This is condition that we impose on $G_0(\vec{R};\omega)^2$ while fixing phases. We start by making a spatial list of the phases as given by the $Arg(z)$ function which restricts the phase obtained to the principal branch $(-\pi,\pi]$. Then, we start at the impurity site for which $\vec{R} = 0$. As we move away from the origin, we multiply phase factors of $e^{i2m\pi}$ to $G_0(\vec{R};\omega)^2 = |G_0(\vec{R};\omega)^2|e^{i\phi_{principal}}$ for all $\vec{R}$ and the m's are so chosen that if $|\vec{R}'| > |\vec{R}|$ then $\phi'_{principal} + 2\pi m' > \phi_{principal} + 2\pi m$. We implemented the choosing of m's in the following way :

1) Define a monotoniser function that takes two arguments that lie between $(-\pi,\pi]$ and keeps adding 2π to the second argument till it becomes greater than the first argument. $mono(x,y)$: Do $y = y + 2\pi$ Till $y > x$.

The following steps are done in each of the symmetry-related octants in space and we write down the steps for the octant $y > 0$ and $x > y$.

2) Start at origin $(0,0)$. Move a step along x-axis to $(x,y) = (1,0)$. Then, $mono(\phi_{principal}(\vec{R} = (x-1,y)), \phi_{principal}(\vec{R} = (x,y))$.

3) Then do $mono(\phi_{principal}(\vec{R} = (x,y)), \phi_{principal}(\vec{R} = (x,y+1))$ along y-direction till $y = x$.

4) Move a step along x-axis. Do $mono(\phi_{principal}(\vec{R} = (x-1,y)), \phi_{principal}(\vec{R} = (x,0))$ where the y of the first argument is highest integer such that $x > \sqrt{(x-1)^2 + y^2}$.

5) Repeat step 3) and 4) till the whole octant is covered.

Similar phase fixing is done for all the octants. Once this is done, the phase of $G_0(\vec{R};\omega)$ is just half that of the phase-fixed $G_0(\vec{R};\omega)^2$. Since, the phase of $G_0(\vec{R};\omega)^2$ has been made well-behaved, the phase of $G_0(\vec{R};\omega)$ will also be well-behaved which is what was desired. In Fig. 7, we show the result of doing the phase-fixing to numerically calculated $G_0(\vec{R};\omega)^2$ and also directly to $G_0(\vec{R};\omega)$ and find that they are in the correct ratio of two.

Proof of self-energy relation

In this section we prove that the relation between the electron and hole lifetimes, $\eta_{hole}(-\omega) = -\eta_{electron}(\omega)$. We will do this using the 2x2 Matsubara formalism. In this formalism, the Green's function for the non-lifetime broadened system in the normal state(i.e. no superconductivity) looks like

$$G_0(k;i\omega_n)^{-1} = \begin{pmatrix} i\omega_n - \epsilon(k) & 0 \\ 0 & i\omega_n + \epsilon(k) \end{pmatrix} \tag{27}$$

where $\omega_n = (2n+1)\pi T$ is the fermionic Matsubara frequency.

We will first prove the relation in the case of the normal electrons coupled to phonons. The self-energy in this case looks like

$$\Sigma(\vec{k};i\omega_n) \;=\; -\frac{T}{N_L}\sum_{\vec{p},\Omega_m} g(\vec{k}-\vec{q},\vec{q})g(\vec{k},-\vec{q})D(\vec{q};i\Omega_m)\tau_3 G_0(\vec{k}-\vec{q};i\omega_n - i\Omega_m)\tau_3 \tag{28}$$

where $\Omega_m = 2m\pi T$ is the bosonic Matsubara frequency, τ_3 is the third componenet of Pauli matrices in the Nambu space, $D(\vec{q};i\Omega_m)$ is the fourier-transform of the phonon's Green's function $D(\vec{q};\tau) = -<T_\tau[A(\vec{q};\tau)A(-\vec{q};0)]>$ and evaluates to

$$D(\vec{q};i\Omega_m) = \frac{1}{2}\left(\frac{1}{i\Omega_m - \Omega_{\vec{q}}} - \frac{1}{i\Omega_m + \Omega_{\vec{q}}}\right) \tag{29}$$

where $\Omega_{\vec{q}}$ is the phonon dispersion. It has the following property : $D(\vec{q};i\Omega_m) = D(\vec{q};-i\Omega_m)$. The $g(\vec{k},\vec{q})$ is the electron-phonon coupling strength coming from the electron-phonon interaction term

$$H_{el-ph} = \frac{1}{N_L}\sum_{\vec{k},\vec{q},\sigma} g(\vec{k},\vec{q})c^\dagger_{\vec{k}+\vec{q},\sigma}c_{\vec{k},\sigma}A_{\vec{q}}. \tag{30}$$

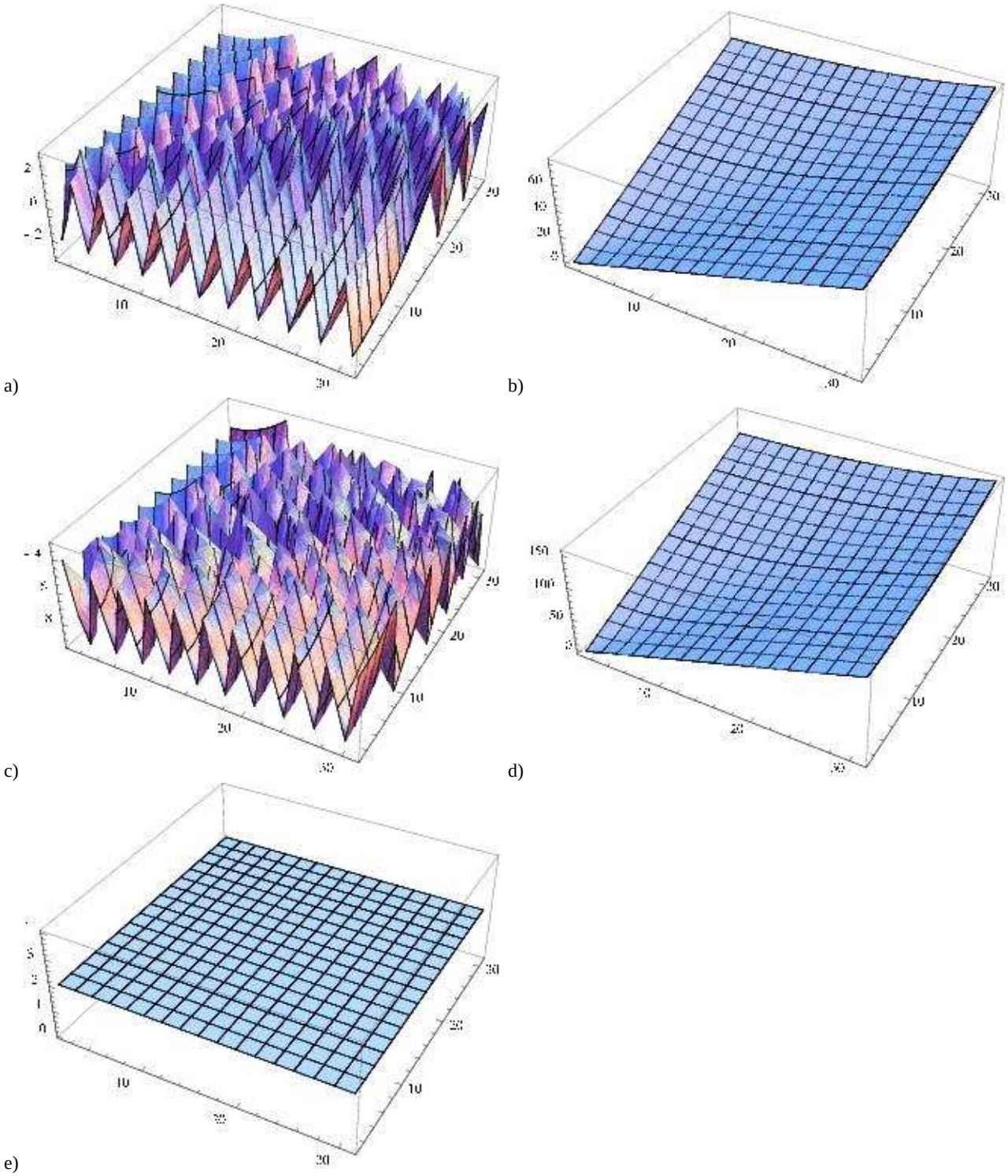

FIG. 7: In these figures, we show the results of the Phase reconstruction algorithm. In a) and c), we show the phase (as a function of space around one quadrant of the impurity at origin) as evaluated using $Arg(z)$ which restricts the values to one branch of the Argument function for $G_0(\vec{R};\omega)$ and $G_0(\vec{R};\omega)^2$ respectively. In b) and d), we show the monotonised phase according to the algorithm described in this section. In e), we confirm that the ratio of the reconstructed phases of $G_0(\vec{R};\omega)^2$ and $G_0(\vec{R};\omega)$ is identically two everywhere. In this example, $\epsilon(\vec{k}) = -2(Cos[k_x] + Cos[k_y])$ and $\eta(\vec{k}) = 0.25 + 0.1(Cos[k_x] + Cos[k_y])$ and $\omega = -1$.

Using the property $D(\vec{q}; i\Omega_m) = D(\vec{q}; -i\Omega_m)$ and $\Omega_{-m} = -\Omega_m$, we can show that(suppressing momenta indices)

$$\begin{aligned}
\Sigma_{22}(-i\omega_n) &\propto \sum_{\Omega_m} \frac{D(\Omega_m)}{-i\omega_n - i\Omega_m + \epsilon} \\
&= \ldots + \frac{D(\Omega_{-1})}{-i\omega_n - i\Omega_{-1} + \epsilon} + \frac{D(\Omega_0)}{-i\omega_n + \epsilon} + \frac{D(\Omega_1)}{-i\omega_n - i\Omega_1 + \epsilon} + \ldots \\
&= \ldots + \frac{-D(\Omega_{-1})}{i\omega_n + i\Omega_{-1} - \epsilon} + \frac{-D(\Omega_0)}{i\omega_n - \epsilon} + \frac{-D(\Omega_1)}{i\omega_n + i\Omega_1 - \epsilon} + \ldots \\
&= \ldots + \frac{-D(\Omega_1)}{i\omega_n - i\Omega_1 - \epsilon} + \frac{-D(\Omega_0)}{i\omega_n - \epsilon} + \frac{-D(\Omega_{-1})}{i\omega_n - i\Omega_{-1} - \epsilon} + \ldots \\
&= -\sum_{\Omega_m} \frac{D(\Omega_m)}{i\omega_n - i\Omega_m - \epsilon} \\
&\propto -\Sigma_{11}(i\omega_n)
\end{aligned} \tag{31}$$

Thus, by analytic continuation, $\Sigma_{22}(-z) = -\Sigma_{11}(z)$ where Σ_{22} and Σ_{11} are the hole and electron self-energies respectively. Thus when we analytically continue till $z = \omega + i\delta$ where ω is real, we see that $\Sigma_{22}(-\omega - i\delta) = -\Sigma_{11}(\omega + i\delta)$. From the analytic properties of Self-energy $\Sigma(\vec{p}; \omega \pm i\delta) = \delta\mu(\vec{p}; \omega) \mp \frac{i}{2}\eta(\vec{p}; \omega)$(see e.g., Eqn. 82 in Vinay Ambegaokar's Chapter on The Green's Function Method in Superconductivity, Vol 1, edited by R. D. Parks), we conclude that

$$\eta_{hole}(-\omega) = -\eta_{electron}(\omega) \ldots QED \tag{32}$$

Also, the chemical potential shift is equal for both holes and electrons. This proof can be extended to higher orders in the electron-phonon coupling by noticing that all higher order terms contributing to self-energy contain odd number of fermion propagators, thus allowing the same kind of manipulation done above to go through analogously. This proof extends to other bosonic modes(e.g. spin wave modes) too since their propagators also satisfy $D(\vec{q}; i\Omega_m) = D(\vec{q}; -i\Omega_m)$. This proof also extends to the case of lifetime broadening induced by electron-electron interaction by the same token that the self-energy terms always have odd number of fermion propagators.

---

* Electronic address: sp384@cornell.edu

[1] P. T. Sprunger *et al.*, Science 275, 1764 (1997); L. Petersen *et al.*, Phys. Rev. B 57, R6858 (1998).

[2] T. Valla *et al.*, Phys. Rev. Lett. 83, 20852088 (1999).

[3] L. Bürgi *et al*, Phys. Rev. Lett. 82, 45164519 (1999); O. Jeandupeux *et al*, Phys. Rev. B 59, 15926 (1999).

[4] I. Adawi, Phys. Rev. 146, 379 (19660.

[5] Yang H.-B. *et al.*, Nature, 456 (2008) 77.

[6] J. W. Alldredge *et al*, Nature Physics 4, 319 - Apr 2008.

[7] It is this "renormalized" dispersion that is measured in FT-STS and ARPES.

[8] Green's functions and condensed matter, G. Rickayzen, Academic Press, 1980.

[9] Q.-H. Wang and D.-H. Lee, Phys. Rev. B 67, 020511 (2003).

[10] K. McElroy *et al*, Nature 422, 592 (2003) and T. Hanaguri *et al.*, Nature Phys. 3, 865 (2007) on BSSCO; J. Lee *et al.*, Nature Physics 5, 800 - September 2009 on Ruthenates.

[11] Practically, even though the LDOS might not be exactly zero outside the bandwidth, we saw that if the spectral weight of the spectrum within the bandwidth is approximately greater than 0.95, which can be expected to be true for well-defined quasiparticles, the Kramers-Kroning essentially works. Moreover, as we show in Fig. 1, this issue matters even less for an energy range much smaller than the bandwidth.

[12] The knowledge of the dispersion can serve as a guide in this regard. Furthermore, we can have an iterative set-up where the result of the analysis scheme using the extrapolated full-bandwidth LDOS data can be used to make a new and better extrapolation to ensure convergence.

[13] Optical excitations in electron microscopy, F. J. Garca de Abajo, Rev. Mod. Phys., 82, 209 (2010).

[14] Our implementation of the Cost function is as follows : $Cost(\{z_r\}) = \sum_r \frac{|z_{r+1} + z_{r-1} - 2z_r|^2}{|(z_{r+1} + z_{r-1})/2|^2}$ for a one-dimensional list $\{z_r\}$, and a suitable extension to two dimensions (see Supplementary).

[15] This can most simply be seen by looking at the equation of motion for a non-interacting Green's function on the continuum(Fourier transformed with respect to time) : $(\zeta + \nabla^2/2m)G_0(R;\zeta) = \delta(R)$. Thus, $G_0(R;\zeta)$ is differentiable for $R \neq 0$. At $R = 0$, $G_0(R;\omega)$ can be non-differentiable, and this manifests as a kink in the phase of Green's function at $R = 0$ for both continuum and lattice. (See Supplementary for a discussion on how this argument applies to the interacting case).

[16] S. Graser, P.J. Hirschfeld, D.J. Scalapino, Phys. Rev. B 77, 184504 (2008)
[17] K. Kanisawa *et al*, Phys. Rev. Lett. 86, 3384 (2001).
[18] A. Weismann *et al*, Science 323, 1190 (2009).
[19] W. D. Wise *et al*, Nature Physics, Volume 5, Issue 3, pp. 213-216 (2009)
[20] S. Pujari and C. L. Henley, Phys. Rev. B 82, 035109 (2010).